# Improved Grain Boundary Conductivity By Post Annealing: Minimizing Vacancy Depletion through Non-Equilibrium Distribution of Immobile Species

ECS Transactions, 61 (1) 139-150 (2014)
10.1149/06101.0139ecst ©The Electrochemical Society

# Improved Grain Boundary Conductivity by Post Annealing: Minimizing Vacancy Depletion through Non-Equilibrium Distribution of Immobile Species

Lei Zhang, Liangzhu Zhu, Feng Liu, and Anil V. Virkar

Department of Materials Science and Engineering, University of Utah, Salt Lake City, UT 84112, USA

A one dimensional model has been used to study the thermodynamics of defects in ionic crystals. It is found that space charge layer near grain boundary contributes to grain boundary resistance. Quenching less mobile ions to a distribution equilibrated at higher annealing temperatures increases point defect concentrations, which leads to a smaller grain boundary resistance. EIS measurement confirmed the model, and it is found that post annealing at higher temperatures helps to improve ionic transport through grain boundary.

## Introduction

Typical electrolyte materials in solid oxide fuel cells (SOFC) and solid oxide electrolyzer cells (SOEC) are yttria-stabilized zirconia (YSZ), Sr and Mg-doped $LaGaO_3$ (LSGM) or doped cerium oxide. These solid oxides exhibit good oxygen ion conductivity at elevated temperatures, typically above 600°C. It is preferable to lower the operating temperature to 600°C, and possibly even lower. During the last two decades, considerable effort has been devoted to lower the ohmic resistance, primarily by using thin electrolyte film, anode-supported cell design. On the other hand, much effort has also been devoted to lowering the cathode polarization resistance. This has led to the development of a number of excellent cathodes, so that at least in many cell designs, the cathode is no longer the component which limits cell performance. Our recent work [1] has shown that the ohmic loss may actually be the dominant loss even in anode-supported thin electrolyte cells, necessitating additional efforts to further reduce the ohmic contribution to the net cell resistance. It is known that at low temperatures, the ceria electrolyte resistance is dominated by grain boundary resistance (shown in Figure 1), which in turn is often dictated by space charge effects. In YSZ also, resistance at low temperatures is often dominated by grain boundaries.

The purpose of the present work was to examine the role of space charge on grain boundary contribution to the electrolyte resistance. Kliewer and Koehler [2] studied the origin of space charge at grain boundaries in pure NaCl and $CaCl_2$-doped NaCl. They found that space charge was a result of charge neutrality and formation energy difference between cation and anion vacancy. Guo [3] applied Kliewer and Koehler's method to give a quantitative description of space charge in YSZ. Lee [4] studied distributions of dopants and vacancies in YSZ by treating space charge layer like that in semiconductor. In the present work, Kliewer and Koehler's [2] approach will be followed.

## Theory and Simulation Details

The simplest ionic crystal is NaCl, which has a Halite structure. Space charge layer in pure NaCl crystal is first reviewed. Considering $CaCl_2$ doped NaCl, the effect of dopant on space charge layer is reviewed. Finally, the same approach will be applied to YSZ.

The case of Pure NaCl

As described in Kliewer and Koehler's work [2], the crystal is considered to have two surfaces in x direction and to be infinite in y and z directions, so the problem is one dimensional. The electrostatic potential $\Phi(x)$ which arises from vacancy distributions in the crystal follows Poisson's equation (1) with dielectric constant ε of this crystal [2].

$$\nabla^2\Phi(x) = d^2\Phi(x)/dx^2 = -4\pi\rho(x)/\varepsilon \quad (1)$$

where $\rho(x)$ is the charge density with the following expression.

$$\rho(x) = e\{n_a(x) - n_c(x)\} \quad (2)$$

with $n_a(x)$ and $n_c(x)$ to be anion and cation vacancy concentrations, respectively. The boundary conditions are

$$\Phi\big|_{x=0} = \Phi\big|_{x=2L} = 0 \quad (3)$$

$$d\Phi/dx\big|_{x=L} = 0 \quad (4)$$

Assuming the ionic crystal is in a state of thermal equilibrium, which is determined by minimization of Helmholtz free energy F of the crystal. The free energy per unit area of the half of the disordered crystal is [2]

$$F = \int_0^L dx\left[n_c(x)F_c + n_a(x)F_a + n_B(x)\{F_c + F_a - B\} + \tfrac{1}{2}\rho(x)\Phi(x)\right] - TS_c \quad (6)$$

where $F_c$ and $F_a$ are the cation and anion vacancy formation energy, respectively. $n_B(x)$ is the concentration of paired (bound) cation and anion vacancies, and B is the binding energy between cation and anion vacancies. $S_c$ is the configurational entropy.

At thermal equilibrium state, the variation of equation (6) should be zero, which gives [2]

$$n_c(x) = N\exp\{-(F_c - e\Phi(x))/kT\} \quad (7A)$$

$$n_a(x) = N\exp\{-(F_a + e\Phi(x))/kT\} \quad (7B)$$

$$n_B(x) = Nz_n\exp\{-(F_c + F_a - B)/kT\} \quad (7C)$$

where $z_n$ is the number of nearest unlike neighbors[2].

Combining equation (1), (2) and (7), governing equation of electrostatic potential is

$$\frac{d^2\Phi(x)}{dx^2} = -\frac{4\pi eN}{\varepsilon}\left[\exp\left\{-\frac{F_a + e\Phi(x)}{kT}\right\} - \exp\left\{-\frac{F_c - e\Phi(x)}{kT}\right\}\right] \quad (8)$$

A numerical solution to (8) is given in the present work using Matlab. Once $\Phi(x)$ is known, both cation vacancy and anion vacancy distributions can be determined. The above discussion assumes thermal equilibrium for both cation vacancies and anion vacancies. However, it is known that $Na^+$ ion is more mobile than $Cl^-$ ion. Seitz mentioned in a review [5] that chloride ions carry about 7% of the ionic current in NaCl crystal at 900 K. Therefore, the diffusivity of $Na^+$ ion is about 13 times larger than that of

$Cl^-$ ion. Considering the larger activation energy for $Cl^-$ ion diffusion, the ratio between diffusivity of $Na^+$ ion and $Cl^-$ ion should be even larger at lower temperatures. Therefore, it will take much longer time for $Cl^-$ ion to reach equilibrium distribution than it does for $Na^+$ ion. This enables adjusting ionic conductivity in ionic crystals by post annealing.

Suppose there are two NaCl crystals, sample 1 and sample 2, that are both at thermal equilibrium at 700 K. At this temperature, the conductivity of $Na^+$ ion is about $10^{-5}$ S/cm[6], and $Cl^-$ ion is sluggish and may be treated as immobile. Now sample 1 is kept at 700 K, while sample 2 is annealed at 1000 K and then quenched to 700 K. In sample 2, $Cl^-$ ion still maintains its equilibrium distribution at 1000 K, while $Na^+$ ion quickly reaches its new equilibrium distribution at 700 K. Due to the differences in $Cl^-$ ion distributions in the two samples, it is reasonable that $Na^+$ ion distribution will also be different. Therefore, thermal history is expected to have an influence on ionic conductivity in ionic crystals.

$$\frac{d^2\Phi^{1000}(x)}{dx^2} = -\frac{4\pi eN}{\varepsilon}\left[\exp\left\{-\frac{F_a + e\Phi^{1000}(x)}{k(1000K)}\right\} - \exp\left\{-\frac{F_c - e\Phi^{1000}(x)}{k(1000K)}\right\}\right] \quad (9)$$

$$n_a^{1000}(x) = N\exp\left\{-\frac{F_a + e\Phi^{1000}(x)}{k(1000K)}\right\} \quad (10)$$

$$\frac{d^2\Phi^{700}(x)}{dx^2} = -\frac{4\pi eN}{\varepsilon}\left[n_a^{1000}(x) - \exp\left\{-\frac{F_c - e\Phi^{700}(x)}{k(700K)}\right\}\right] \quad (11)$$

Equation (9), (10) and (11) demonstrate that when anion vacancy maintains its equilibrium distribution at 1000 K, the cation vacancy equilibrium distribution at a lower temperature will be different from that when both species reach equilibrium.

The Case of $CaCl_2$ Doped NaCl

Doping is an effective way to adjust ionic conductivity by changing vacancy concentration. In the present work, Kliewer and Koehler's approach is followed [2].

Suppose pure NaCl is doped with $CaCl_2$ at an average concentration of C. Now, there will be two more species that contribute to total free energy of the crystal. One is isolated $Ca_{Na}^{\bullet}$ point defect having one positive charge, and its concentration is denoted as $n_{if}$; the other is the paired neutral defect consisting of $Ca_{Na}^{\bullet}$ and cation vacancy with binding energy of $B_i$, and its concentration is denoted as $n_{ib}$. Now equation (6) becomes [2]

$$F = \int_0^L dx\left[n_c(x)F_c + n_a(x)F_a + n_B(x)\{F_c + F_a - B\} + n_{ib}(x)\{F_c - B_i\} + \tfrac{1}{2}\rho(x)\Phi(x)\right] - TS_c \quad (12)$$

and equation (2) becomes

$$\rho(x) = e\{n_{if}(x) + n_a(x) - n_c(x)\} \quad (13)$$

By setting the variation of equation (12) to zero, we have [2]

$$n_c(x) = N\exp\{-(F_c - e\Phi(x))/kT\} \quad (14A)$$

$$n_a(x) = N\exp\{-(F_a + e\Phi(x))/kT\} \quad (14B)$$

$$n_B(x) = Nz_n\exp\{-(F_c + F_a - B)/kT\} \quad (14C)$$

$$n_{if}(x) = N \exp\{-(e\Phi(x) + \alpha)/kT\} \quad (14D)$$

$$n_{ib}(x) = Nz_{nn} \exp\{-(F_c - B_i + \alpha)/kT\} \quad (14E)$$

where $z_{nn}$ is the number of nearest like neighbors, and $\alpha$ is a Lagrange multiplier introduced by the fact that total number of dopant is fixed.

$$\int_0^L dx\left(n_{if}(x) + n_{ib}(x)\right) = NCL \quad (15)$$

Combining equations (1), (13), (14) and (15), electrostatic potential distribution can be solved, and therefore the equilibrium distribution of each species is known.

The Case of YSZ

Pure cubic $ZrO_2$ has a stable fluorite structure at high temperature. By doping with 8 mole percent of $Y_2O_3$, the cubic structure is stabilized at room temperature. There are even more species which contribute to total free energy of the crystal. They are $V_O^{\bullet\bullet}$, $V_{Zr}^{''''}$, $Y_{Zr}^{'}$, $V_O^{\bullet\bullet} + V_{Zr}^{''''}$, $2V_O^{\bullet\bullet} + V_{Zr}^{''''}$, $V_O^{\bullet\bullet} + Y_{Zr}^{'}$ and $V_O^{\bullet\bullet} + 2Y_{Zr}^{'}$.

According to Bjerrum theory of ion association, most bonded point defects are neutral pairs like $2V_O^{\bullet\bullet} + V_{Zr}^{''''}$ and $V_O^{\bullet\bullet} + 2Y_{Zr}^{'}$. Therefore, $V_O^{\bullet\bullet} + V_{Zr}^{''''}$ and $V_O^{\bullet\bullet} + Y_{Zr}^{'}$ are neglected. By defining $n_c(x)$, $n_a(x)$, $n_{if}(x)$, $n_B(x)$ and $n_{ib}(x)$ to be respectively concentrations of $V_{Zr}^{''''}$, $V_O^{\bullet\bullet}$, $Y_{Zr}^{'}$, $2V_O^{\bullet\bullet} + V_{Zr}^{''''}$ and $V_O^{\bullet\bullet} + 2Y_{Zr}^{'}$, the total free energy of the YSZ crystal exhibits similar expression as equation (12). The effective charge on the free point defects ($V_{Zr}^{''''}$, $V_O^{\bullet\bullet}$ and $Y_{Zr}^{'}$) are -4, +2 and -1, respectively. So equation (13) becomes

$$\rho(x) = e\{2n_a(x) - n_{if}(x) - 4n_c(x)\} \quad (16)$$

Set the variation of equation (12) to be zero, we have

$$n_c(x) = N_c \exp\{-(F_c - 4e\Phi(x))/kT\} \quad (17A)$$

$$n_a(x) = N_a \exp\{-(F_a + 2e\Phi(x))/kT\} \quad (17B)$$

$$n_B(x) = N_c z_n \exp\{-(F_c + 2F_a - B)/kT\} \quad (17C)$$

$$n_{if}(x) = N_c \exp\{-(-e\Phi(x) + \alpha)/kT\} \quad (17D)$$

$$n_{ib}(x) = N_a z_{nn} \exp\{-(F_c - B_i + \alpha)/kT\} \quad (17E)$$

where $N_c$ and $N_a$ are the lattice site density of cation and anion.

Since in each paired $V_O^{\bullet\bullet} + 2Y_{Zr}^{'}$, there are two $Y_{Zr}^{'}$, equation (15) becomes

$$\int_0^L dx\left(n_{if}(x) + 2n_{ib}(x)\right) = N_c CL \quad (18)$$

Combining equation (1), (16), (17) and (18), electrostatic potential distribution can be solved, and therefore the equilibrium distribution of each species is known.

Simulation Details

Differential equation (1) together with boundary value conditions (3) and (4) forms a one dimensional boundary value problem (BVP). BVP for pure NaCl is solved simply using the bvp4c solver embedded in Matlab [7]. In BVPs for doped NaCl and YSZ, the existence of Lagrange multiplier requires a self-consistent calculation, which is also realized using Matlab. Parameters in the simulation are summarized in Table I.

## Experiment Details

Pellets of YSZ powder of composition 92 mol.% $ZrO_2$ – 8 mol.% $Y_2O_3$ were die-pressed and sintered in air at 1600°C for 2 h. The typical thickness of the pellets was ~1.4 mm. Pt paste was applied on both sides of the pellets and fired at 800°C in air for 1 h. The diameter of the electrode was ~13 mm.

Post annealing was done in a high temperature tube furnace. Once cations and anions reached their equilibrium distributions at the annealing temperature, the sample was taken out of the furnace in less than 5 seconds. Therefore, cation vacancy concentration was frozen. It is known that cation vacancies are essentially immobile compared to oxygen vacancies. The duration of annealing was determined by equation (19)

$$L_{gb} = 2\sqrt{Dt} \tag{19}$$

where $L_{gb}$ is the space charge layer thickness, D is the diffusion coefficient of the slowest ion ($Zr^{4+}$ in this case), t is the duration. Kilo has measured D in YSZ using $Zr^{96}$ tracer [8]. Assuming $L_{gb}$ to be 0.1 μm, duration of annealing is calculated (summarized in Table II).

Electrochemical impedance spectroscopy (EIS) was used to measure spectra on the samples in air over temperatures ranging from 300°C to 400°C in 20 degree intervals using the four terminal method. The impedance measurements were conducted using Solartron 1260 Frequency Response Analyzer over a frequency range between 10 Hz and 1 MHz. The stray impedance is considered and treated in the way described elsewhere [9].

## Results and Discussion

NaCl at Thermal Equilibrium

The BVP composed of equation (8), (3) and (4) was solved by simply using bvp4c in Matlab. The electrostatic potential distribution from grain boundary to grain interior is shown in Figure 2A. The potential at x=0 is fixed to be zero by boundary condition (3). At x=L, the derivative of potential is zero due to the symmetry of the model; while, the potential saturates at a value of -0.26 V. Charge neutrality is required at the grain interior if the crystal is large enough. Therefore, equation (7A) and (7B) should be equal where far from the grain boundary. This gives [2]

$$\exp\{-(F_c - e\Phi(\infty))/kT\} = \exp\{-(F_a + e\Phi(\infty))/kT\} \tag{20}$$

As a result,

$$e\Phi(\infty) = \tfrac{1}{2}(F_c - F_a) \tag{21}$$

From Table I, $F_c$ is 0.8 eV, and $F_a$ is 1.32 eV. Therefore, $\Phi(\infty)$ has a value of -0.26.

Following equation (7A) and (7B), cation vacancy concentration distribution and anion vacancy concentration distribution were obtained and are summarized in Figure 2B and Figure 2C. The calculation was done at chosen temperatures of 800 K, 900 K, 1000 K and 1074 K. It is clear that as temperature increases, space charge layer becomes thinner, and vacancy concentration goes higher. This is consistent with Boltzmann distribution.

NaCl after Post Annealing

The solution to the BVP composed of equations (9), (11), (3) and (4) was calculated at 800 K in such a way that anion vacancy concentration was fixed at its equilibrium concentration corresponding to the annealing temperature (800 K, 900 K, 1000 K and 1074 K) and cation vacancy was allowed to relax at 800 K. Figure 3 shows the results.

By comparing Figure 2C and 3C, it is clear that anion vacancy concentration at 800 K has maintained its distribution at the corresponding annealing temperature. Figure 3A shows potential distribution is influenced by thermal history. $\Phi(\infty)$ deviates from the value of -0.26 V after annealing. In Figure 3B, cation vacancy concentration at both grain boundary and grain interior increases with annealing at higher temperature.

EIS Measurement on YSZ

The results of EIS measurement at 300 °C are summarized in Figure 4. For each curve, there are three arcs, which, from high frequency to low frequency, correspond to grain interior, grain boundary and electrode. However, since the lowest frequency at which measurement were done was 10 Hz, the electrode arc is not complete, and it only shows a tail. As the annealing temperature increases, the measured grain boundary arc gradually merged with grain interior arc. The values of grain interior resistance and grain boundary resistance can be interpreted using the method described elsewhere [9] and are summarized in Table III.

The sample was annealed sequentially at 1600 °C, 1300 °C and 1200 °C. It is clear that, by annealing at higher temperature, both grain interior and grain boundary resistance decreased. This results from the increased oxygen vacancy concentration.

## Summary

Space charge layer near grain boundary is believed to be the origin of grain boundary resistance [2]. A one dimensional model has been used to study the thermodynamics of defects in ionic crystal. It is found that both thermal history and doping have influence on point defect concentration in space charge layer, which in turn affects grain boundary resistance. EIS measurement confirmed the model, and it is found that post annealing at high temperature helps to improve ionic transport through grain boundary.

## Acknowledgement

This work was supported in part by the US Department of Energy under its Energy Frontiers Research Centers program at the University of Utah as a flow through from the University of South Carolina (HeteroFoam) under Grant Number DE-SC0001061 (work of Lei Zhang), and by the US Department of Energy under Grant Number DE-FG02-06ER46086 (work of Anil Virkar).

## References


[1] L. Zhu, L. Zhang, F. Zhao, A.V. Virkar, *ECS transcription*, 2014

[2] K. Kliewer and J. Koehler, "Space charge in ionic crystals. I. General approach with application to NaCl," *Phys. Rev.*, no. 4, 1965.

[3] X. Guo, "Physical origin of the intrinsic grain-boundary resistivity of stabilized-zirconia: role of the space-charge layers," *Solid State Ionics*, vol. 2738, no. 95, 1995.

[4] J.-S. Lee and D.-Y. Kim, "Space-charge concepts on grain boundary impedance of a high-purity yttria-stabilized tetragonal zirconia polycrystal," *J. Mater. Res.*, vol. 16, no. 09, pp. 2739–2751, Jan. 2001.

[5] F. Seitz, "Color centers in alkali halide crystals. II," *Rev. Mod. Phys.*, vol. 26, no. 1, p. 7, 1954.

[6] C. Pierce, "Effect of hydrostatic pressure on ionic conductivity in doped single crystals of sodium chloride, potassium chloride, and rubidium chloride," *Phys. Rev.*, vol. 123, no. 3, pp. 744–754, 1961.

[7] L. F. Shampine, M. W. Reichelt, and J. Kierzenka, "Solving Boundary Value Problems for Ordinary Differential Equations in MATLAB with bvp4c."

[8] M. Kilo, G. Borchardt, and B. Lesage, "Cation transport in yttria stabilized cubic zirconia: 96Zr tracer diffusion in (ZrxY1-x) O2-x/2 single crystals with $0.15 \leq x \leq 0.48$," *J. Eur. Ceram. Soc.*, vol. 20, pp. 2069–2077, 2000.

[9] L. Zhang, F. Liu, K. Brinkman, K. L. Reifsnider, and A. V. Virkar, "A study of gadolinia-doped ceria electrolyte by electrochemical impedance spectroscopy," *J. Power Sources*, vol. 247, pp. 947–960, Feb. 2014.

Table I: Simulation Parameters

| | $F_c$ (eV) | $F_a$ (eV) | $B_i$ (eV) | $N_c$ ($cm^{-3}$) | $N_a$ (eV) | $Z_n$ | $Z_{nn}$ | ε |
|---|---|---|---|---|---|---|---|---|
| NaCl | 0.8 | 1.32 | | 2.25E22 | 2.25E22 | 6 | | 5.6 |
| NaCl+$CaCl_2$ | 0.8 | 1.32 | 0.4 | 2.25E22 | 2.25E22 | 6 | 12 | 5.6 |

Table II: Annealing time needed to fully relax sluggish $Zr^{4+}$

| T (°C) | T (K) | D ($cm^2s^{-1}$) | t (s) | t (h) | t (day) |
|---|---|---|---|---|---|
| 1600 | 1873 | 4.0E-14 | 6.25E2 | 0.17 | 0.01 |
| 1500 | 1773 | 8.0E-15 | 3.13E3 | 0.87 | 0.04 |
| 1400 | 1673 | 1.3E-15 | 1.92E4 | 5.34 | 0.22 |
| 1300 | 1573 | 1.9E-16 | 1.32E5 | 36.55 | 1.52 |
| 1200 | 1473 | 1.9E-17 | 1.32E6 | 365.5 | 15.23 |
| 1100 | 1373 | 2.0E-18 | 1.25E7 | 3472.22 | 144.68 |
| 1000 | 1273 | 1.0E-19 | 2.50E8 | 69444.44 | 2893.52 |

Table III: $R_0$, $R_g$ and $R_{gb}$ measured using EIS

| T (°C) | Rg (Ω) | Rgb (Ω) |
|---|---|---|
| 1200 | 6725 | 867 |
| 1300 | 5879 | 812.8 |
| 1600 | 5226 | 630.8 |

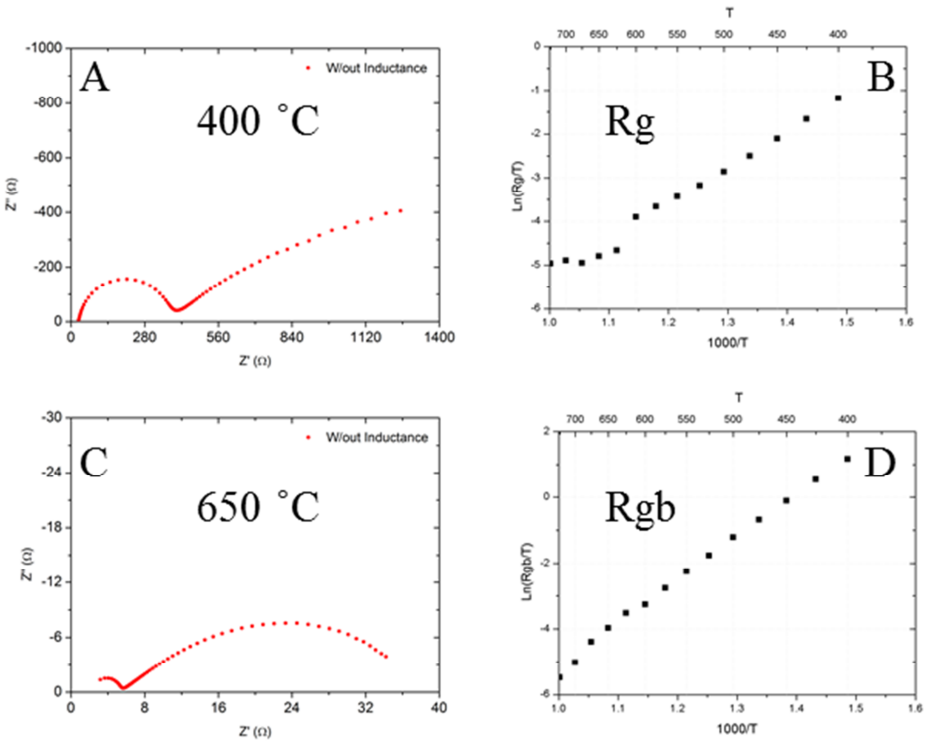


Figure 1A and 1C: Electrochemical impedance spectra on a GDC electrolyte; 1B and 1D: Arrhenius plots of grain and grain boundary resistance. At low temperature, like 400 °C, grain boundary resistance is much larger than grain interior resistance; at high temperature, like 650 °C, grain boundary resistance is still of the same magnitude as grain interior resistance.

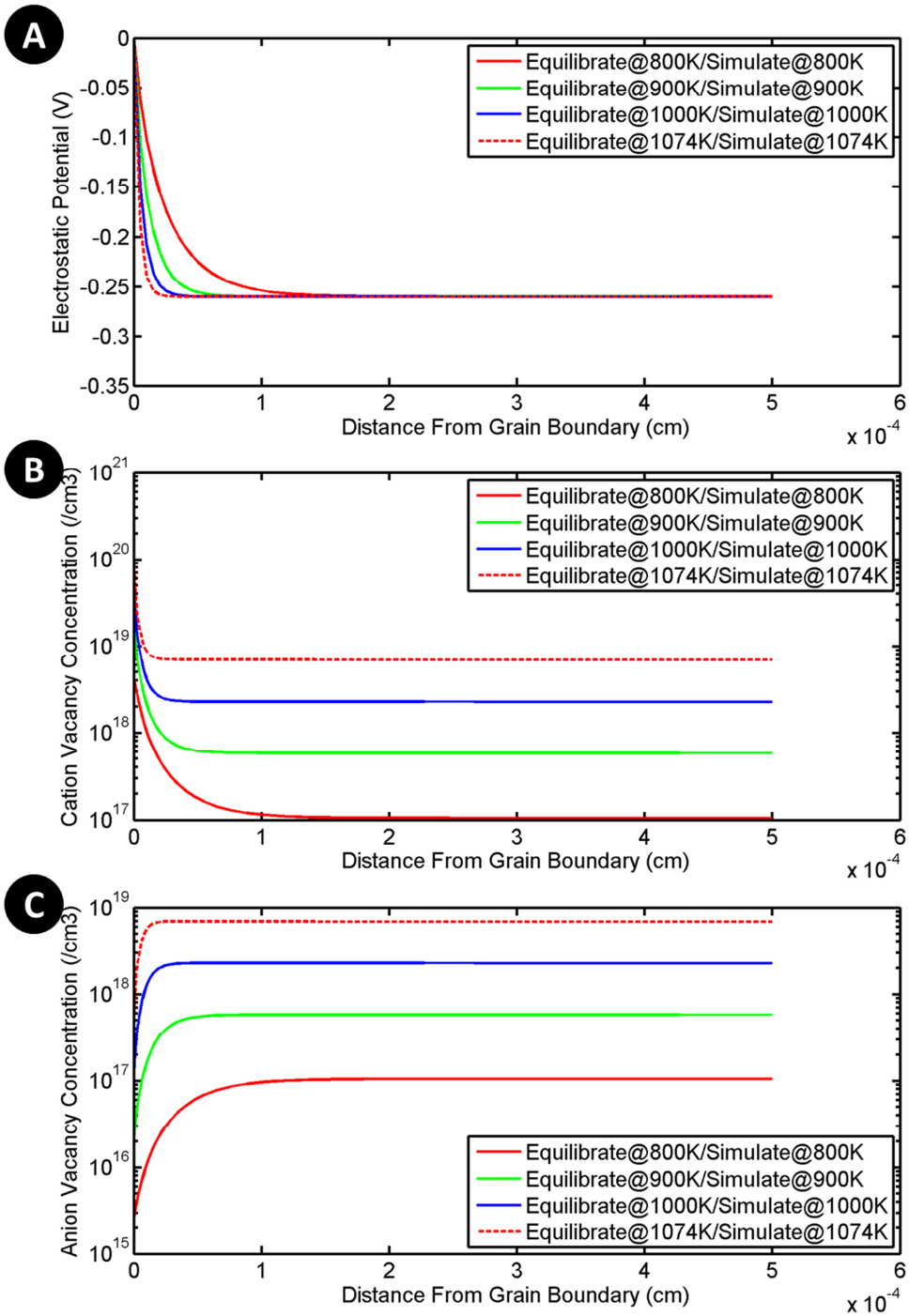


Figure 2A is the electrostatic potential distribution in pure NaCl crystal; 2B and 2C are the concentration distributions of cation vacancy and anion vacancy. As temperature goes up, space charge layer thickness becomes smaller.

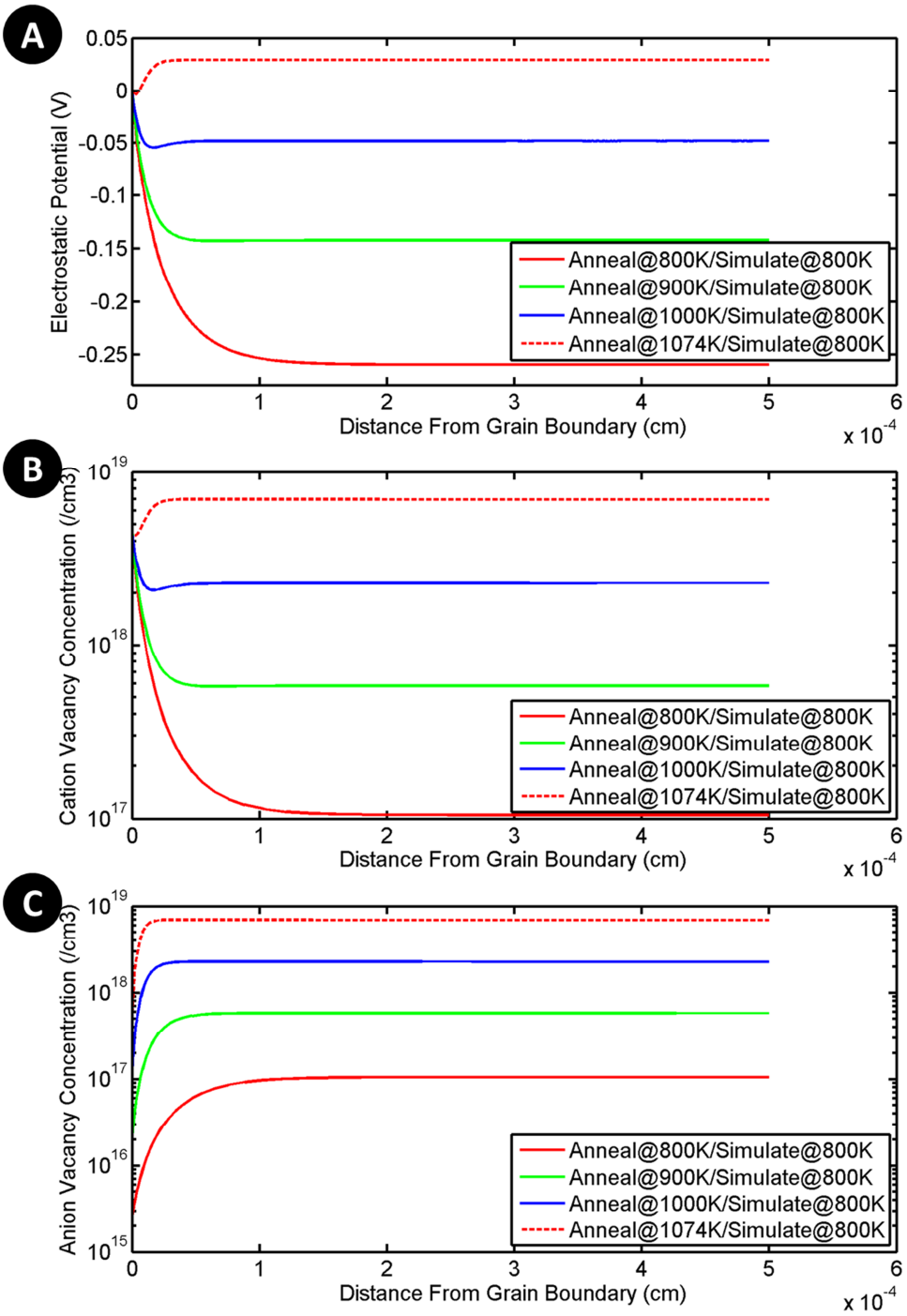


Figure 3A is the electrostatic potential distribution in annealed NaCl crystal; 3B and 3C are the concentration distribution of cation vacancy and anion vacancy. Anion vacancy concentration is fixed to the equilibrium distribution at annealing temperature due to its sluggish diffusivity. As a result, cation vacancy concentration is influenced by the thermal history.

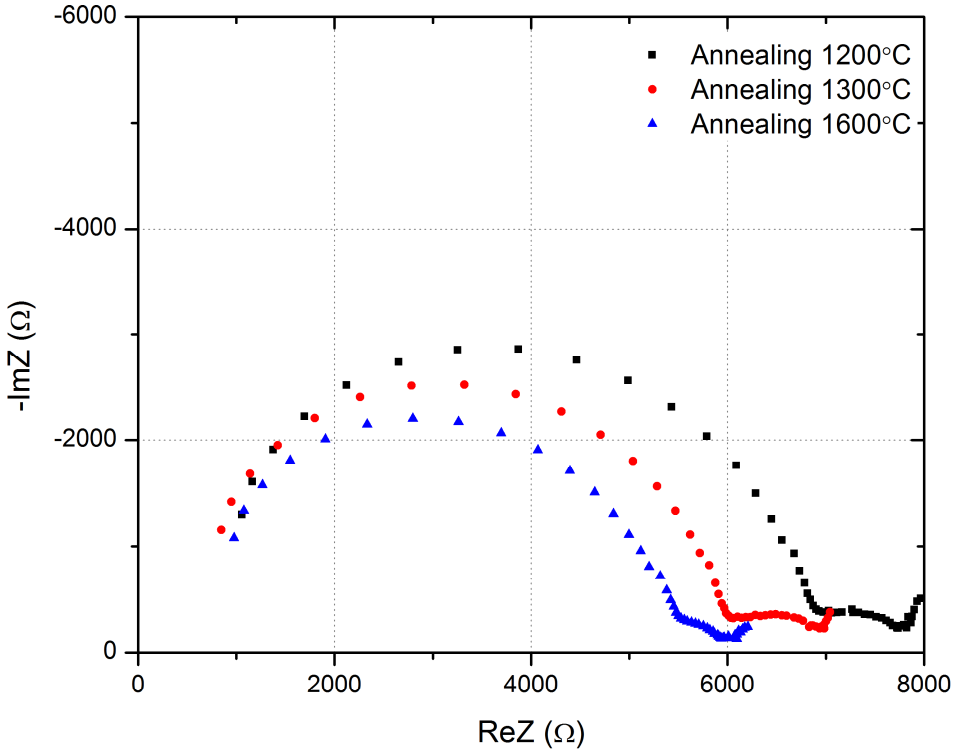


Figure 4 summarizes the EIS measurement results on a YSZ pellet sample. The sample was annealed sequentially at 1600 °C, 1300 °C and 1200 °C. The left intersects of the extrapolated curve with x-axis should be less than 10 Ω. The reason that these intersects are much larger than 10 Ω is stray inductance from both lead and instrument, which is well discussed elsewhere[9]. It is clear that, by annealing at higher temperature, both grain interior and grain boundary resistance decreased.